Analysis of Dark Current Mechanisms for Split-Off Band Infrared Detectors at High Temperatures

Y. F. Lao, P. V. V. Jayaweera, Steven G. Matsik, A. G. Unil Perera, *Senior Member, IEEE*, H. C. Liu, *Fellow, IEEE*, M. Buchanan, and Z. R. Wasilewski

***Abstract*—An analysis of dark current mechanisms has been performed on high-operating-temperature (up to 330 K) split-off (SO) band p^+-GaAs/AlGaAs heterojunction infrared detectors (3–5 μm). In contrast to conventional 1-D current models due to carrier transport based on tunneling and/or thermionic emission mechanisms, a 2-D electrical model is used to explain nonuniformity degradation of zero-bias differential resistance (R_0A) with temperatures as measured on SO detectors. The 2-D characteristic of carrier transport could have the limitation on high-temperature performances of detectors and, hence, needs optimizing. A theoretical model shows that this 2-D effect can be reduced by structural modifications such as using smaller mesa sizes, higher doping of the p^+-GaAs layer, and a higher potential barrier that prospectively provides better electrical uniformity for SO detectors working at high temperatures.**

***Index Terms*—Dark currents, GaAs–AlGaAs, heterojunctions, infrared detectors.**

I. Introduction

THE dependence of carrier transport on operating conditions is one of critical limitations to performances of optoelectronic devices. For example, the detectivity of infrared detectors [1]–[3] is closely related to the operating temperature due to its main effect on dark currents. Understanding the dark current mechanism is hence a primary necessity for detector designing. Owing to its symmetrical geometry such as circular or square configurations, a detector can be generally modeled within a 2-D scheme regarding the electrical characteristics. Further simplifications can be made when working at low temperatures. The main current sources come from carrier surmounting over (thermionic emission) [1], [4] and/or tunneling [1], [5] through potential barriers and are limited by the vertical transportation (in the growth direction), whereas lateral (in-plan) currents can be neglected, provided the in-plan conductivity is high enough. A 1-D consideration can thus be used as detector models [1]–[5]. Recently, a high-operating-temperature (up to 330 K) infrared detector ($3-5$ μm) based on optical transitions between the heavy/light hole band and the spin–orbit split-off (SO) band has been reported [6], [7]. Further optimizations are also possible through theoretical modeling [8]. These investigations demonstrate the potential of SO detectors for uncooled operations. However, a temperature-related effect will become dominant for SO detectors. Carriers have a quicker thermionic escape over the barrier at high temperatures than that at low temperatures, raising the vertical component of conductivity to a level comparable to the lateral one and, thus, the nonnegligible lateral currents. This 2-D transport mode generates possible current localizing effect and, hence, the electrical nonuniformity.

Quantum-well infrared photodetectors (QWIPs) [9] and homojunction [10]/heterojunction [4] detectors are composed of doped active regions for absorbing light and undoped barriers for separating photoexcited carriers from those other than photoactivation. Temperature rising always increases carrier escape over barriers, leading to an increased conductivity ratio of the vertical component to the lateral. In such a situation, currents could become localized with the maxima at the location of metal contact [11]. This issue is critical for high-operating-temperature unipolar detectors as the escape over barriers is always temperature dependent. The 2-D currents could raise the issue of collection-efficiency degradation due to nonuniformity over the entire optical region of detectors and, thus, limit the performances. Previous models have not taken this effect into account.

In this paper, a theoretical model involving the 2-D transport characteristic of carriers was investigated. Current–voltage–temperature (I–V–T) measurements on SO detectors show that R_0A deviation only occurs at high temperatures, indicating a temperature-dependent behavior of electrical uniformity. A critical parameter, i.e., threshold temperature, defined by both experimental and theoretical results, represents the beginning of nonuniformity and needs to be optimized.

II. Experiments

The material parameters of p^+-GaAs/AlGaAs SO infrared detectors are listed in Table I, and a schematic of the device is shown in Fig. 1. All samples were grown on the semi-insulating GaAs substrates and comprised periodic units of p^+-GaAs emitter layers and undoped AlGaAs barriers that were sandwiched between 0.2- and 0.7-μm-thick 1×10^{19} cm^{-3} p^{++}-GaAs. Detectors were processed into four square mesas of 400×400, 600×600, 800×800, and 1000×1000 μm^2 by wet etching techniques. Ti/Pt/Au ohmic contacts were

Manuscript received December 16, 2009; revised March 3, 2010; accepted March 9, 2010. Date of publication April 19, 2010; date of current version May 19, 2010. This work was supported in part by the U.S. Army under Grant W911NF-08-1-0448. The review of this paper was arranged by Editor L. Lunardi.

Y. F. Lao, P. V. V. Jayaweera, S. G. Matsik, and A. G. U. Perera are with the Department of Physics and Astronomy, Georgia State University, Atlanta, GA 30303 USA (e-mail: uperera@gsu.edu).

H. C. Liu, M. Buchanan, and Z. R. Wasilewski are with the Institute for Microstructural Sciences, National Research Council of Canada, Ottawa, ON K1A 0R6, Canada.

Digital Object Identifier 10.1109/TED.2010.2046065

TABLE I
MATERIAL PARAMETERS FOR FOUR p^+-GaAs/AlGaAs PERIODIC STRUCTURES. d_e AND d_b ARE THE THICKNESSES OF THE EMITTER AND BARRIER, RESPECTIVELY. N_e IS THE DOPING CONCENTRATION OF p^+-GaAs. N IS THE NUMBER OF PERIODS WITH $N+1$ BARRIERS

Sample No.	p^+-GaAs emitter		Undoped Al_xGaAs barrier		N periods
	d_e (nm)	N_e (10^{18} cm^{-3})	d_b (nm)	x	
SP1	18.8	3	60	0.28	30
SP2	18.8	3	60	0.37	30
SP3	18.8	3	60	0.57	30

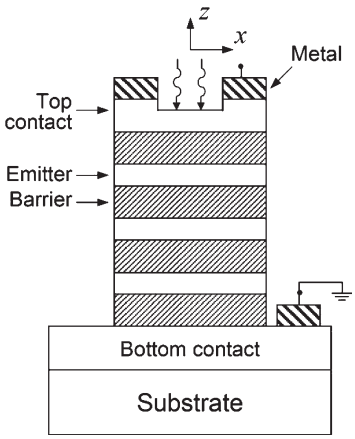

Fig. 1. Structure of SO infrared detectors with square-ring metal electrodes. The emitter layers are highly p-doped GaAs, while the AlGaAs barriers are undoped. The coordinates define the 2-D plane with the z-axis positioned at the device center.

evaporated onto the top and bottom contact layers. A ring metal was used as the top electrode configuration with squares of 260, 460, 660, and 860 μm opened as the optical windows. The top contact layer is partially etched to thin its thickness for optical illumination. I–V characteristics under dark conditions were measured at different temperatures from 40 to 330 K.

III. THEORETICAL MODEL

The current due to carrier transport within a heterostructure can be schematically formulated as

$$\vec{J} = \sum_k q p_k \vec{v}_k \tag{1}$$

where the summation is carried out over the wavenumber k. The vector $\vec{J}$ denotes a 2-D distribution in the cross-sectional plane along the growth axis. q, p_k, and $\vec{v}_k$ are the charge, hole density, and velocity, respectively. The explicit involvement of velocity is a simplification to practical issues of carrier transport and should be expanded to the specific form, depending on involved current mechanisms. For example, in the case of tunneling process, $\vec{v}_k$ should be replaced by $dE(k)/\hbar dk$, and the familiar formula for tunneling current can be deduced [5]. Based on (1), total currents can be described on the summation of two components related to drift–diffusion behavior of carriers along the vertical and lateral directions, respectively. Their contrast determines the transport mode being considered as either 1- or 2-D, which depends on specific conditions as stated in the following.

The evaluation of p_k is straightforward, depending on tunneling and thermionic emission across a potential barrier or simply conduction within a uniform material. The structure of SO infrared detectors with p^+-GaAs/AlGaAs alternative layers and square-ring metal electrodes is shown in Fig. 1. Highly p-doped GaAs layers are responsible for photoabsorption and emitting carriers over the potential barriers. Considering the temperature region where thermionic emission is the dominating source of dark currents, the portion of carriers with higher thermal energy than the potential barrier can move freely on top of the barrier region. $\vec{v}_k$ in (1) can be taken out of the summation as $\vec{v}$, which is described as effective velocity for thermionic carriers. Equation (1) becomes

$$\vec{J} = q\vec{v}\sum_k p_k. \tag{2}$$

This formula is similar to bulk materials where the term $\sum p_k$ represents the emitter contribution to the "effective density" of carriers above barriers. In the lateral direction, bulk parameters are used for current calculation as no barriers appear. From a microscopic point of view, the vertical velocity can be defined as the transfer of carriers across a relevant length within a characteristic transit time τ_{transit} [2]. Theoretically, the evaluation of τ_{transit} is quite complicated as it should include scattering processes (ionized impurity, phonons), impact ionization, recombination, etc. A preferable approach is to use the Monte Carlo simulation method, where either escapes or traps of carriers from the emitter and collected by the contact layer is determined by calculating the probability of various scattering mechanisms. By tracking a large number of carriers, both currents under dark and illumination conditions can be calculated. This method has been successfully used for device modeling and structural optimizing [8], [12]. Here, carrier velocity related to the electrical field is formulated using the following empirical formula [4]:

$$\vec{v} = \frac{\mu\vec{\varepsilon}}{\sqrt{1+(\mu\varepsilon/v_{\mathrm{sat}})^2}} \tag{3}$$

where μ is the low-field mobility, ε represents the electric field, and v_{sat} is the saturation drift velocity. The vertical mobility μ (in later description, it is denoted as μ_z) is actually an effective value due to trapping and emitting of emitters. The current calculated by (2) neglects the contribution from carrier diffusion as only majority holes are considered. By expanding (2), a 2-D current model can be described as follows:

$$\vec{J} = J_x\vec{e}_x + J_z\vec{e}_z \tag{4}$$

$$J_x = \Big[q\left(d_{tc}v_{x(tc)}p_{tc} + d_{bc}v_{x(bc)}p_{bc}\right) + Nqd_ev_{x(e)}p_e + (N+1)qd_bv_{x(b)}\sum_k p_k\Big] \Big/ \sum_i d_i$$

$$J_z = qv_z\sum_k p_k \tag{5}$$

in which v_x and v_z represent velocity components along the lateral $(\vec{e}_x)$ and vertical $(\vec{e}_z)$ directions, respectively, $\sum d_i$ is the total thickness of devices, and N is the number of periods with $N+1$ barriers. The symbols d, v_x, and p for J_x correspond to the thickness, lateral velocity, and hole density for the top contact (tc), bottom contact (bc), emitters (e), and barriers (b), respectively. The formula of J_x was deduced as a weighted average contribution [11] from each layer. A more accurate description can be achieved by handling each layer separately. As verified by numerical calculation in Section IV, this J_x form gives reasonable but direct results to explain experimental measurements. The barrier contribution to conductivity was calculated by treating the carrier concentration as $\sum p_k$. As far as the temperature region for SO detectors is concerned, vertical currents are dominated by thermionic emission over the potential barrier, i.e.,

$$J_z = J_{\mathrm{TE}} = q v_z \int\limits_{k>k_b} f(k) 2d\vec{k}/(2\pi)^3. \tag{6}$$

The summation over k has been replaced by an integral considering the density of states, k_b corresponds to the wavenumber of barrier energy, and $f(k)$ is the Fermi–Dirac distribution function.

It should be noted that lateral currents at low temperatures can be neglected due to equipotential distribution along the in-plane direction. The vertical current [see (6)] is thus a good description for low-temperature operations. This is a result of total currents being fitted to the continuity equation under the steady-state condition, i.e., $\nabla \cdot \vec{J} = 0$, where generation and recombination are neglected due to dark operations. Combined with (4) and (5), the electrical transport equation is derived as a 2-D equation, described as follows:

$$\alpha \frac{\partial^2 \phi}{\partial z^2} + \frac{\partial^2 \phi}{\partial x^2} = 0 \tag{7}$$

where the coordinates are defined as shown in Fig. 1. ϕ is the electric potential, and α is defined as a conductivity ratio of the vertical component to the lateral, i.e.,

$$\alpha \equiv \bar{\sigma}_z / \bar{\sigma}_x \tag{8}$$

$$\bar{\sigma}_x = \Big[q\left(d_{tc}\mu_{x(tc)}p_{tc} + d_{bc}\mu_{x(bc)}p_{bc}\right) + Nqd_e\mu_{x(e)}p_e + (N+1)qd_b\mu_{x(b)}\sum_k p_k \Big] \Big/ \sum_i d_i$$

$$\bar{\sigma}_z = q\mu_z \sum_k p_k. \tag{9}$$

In deducing the above equations, the denominator of (3), is neglected because a low bias (electric field $<$ 1 kV/cm) was applied in experiments. μ_x is a bulk mobility for each layer, while μ_z is an effective value with a temperature-dependent fashion and is, thus, difficult to be calculated. Since dark currents can be exactly modeled using (6) at low temperatures (explained in the following part), it is convenient to extract $\overline{\sigma}_z$ from experimental measurements. The space charge effect is not explicitly considered, which mainly comes from the excess or deficit of cold carriers in the emitters and ionized impurities in the barriers [12], [13]. Its influence could be small due to conduction through major holes. On the other hand, the space charge has an effect on the change of potential shape [13] and can be simply considered as a modification to the shift of thermal activation energy. By following a fitting routine, this modification is actually involved.

At low temperatures, the ratio α is very small (due to exponentially reduced vertical conductivity). Equation (7) can be approximated to $\partial^2\phi/\partial x^2 = 0$, leading to equipotential lateral distribution (being satisfied to the boundary conditions). The 1-D thermionic current exactly represents the I–V characteristics under dark conditions. As the vertical conductivity is temperature sensitive in a behavior of $\exp[-\Delta/k_BT]$, where Δ is the thermal activation energy, the ratio α will be considerably increased with temperatures. The 2-D electric potential with the minimum at device center will decrease the overall collection efficiency on carriers. For this reason, a 2-D electrical analysis on high-operating-temperature SO detectors is necessary. The evaluation of temperature-dependent α, indicating a threshold temperature (denoted by T_t) above which lateral transport takes effect, will be considered. It will be demonstrated that T_t agrees well with measured operating temperatures for optimum SO response. Related optimizing designs are then presented.

IV. Results and Discussion

Under low-bias operation (e.g., electric field $<$ 1 kV/cm), the thermionic current [see (6)] is coincident with Ohm's law due to the negligible denominator of (3) and the image-force effect on the thermal activation energy. Equation (6) is linearly proportional to bias, and the R_0A product can be defined as

$$R_0A = \left(\frac{\partial J_{\mathrm{TE}}}{\partial V}\right)^{-1}\Bigg|_{V=0} \equiv \sum_i d_{bi}/\bar{\sigma}_z \tag{10}$$

where A is the mesa area of devices, and $\sum d_{bi}$ is the total thickness of barriers. For vertical currents, no potential difference on emitters is assumed. The above formula implicitly includes a term $\exp[\Delta/k_BT]$, which comes from the integral in (6). In the experiments, R_0A is calculated from I–V data and should be consistent with the (10) only at low temperatures (still dominated by thermionic currents). The 2-D current mode, leading to R_0A deviation from (10), could take place at high temperatures as analyzed in Section III.

Fig. 2 shows plots of $\mathrm{Log}[R_0A]$ versus $1000/T$ as measured on samples listed in Table I. The cross-sectional geometry area has been used to calculate R_0A. At the low-temperature side of curves, the R_0A product is the same for different mesa sizes, indicating uniform currents within devices. So the cross-sectional geometry area represents the actual conduction area. The R_0A–T curve can be well fitted by (10) (the solid line). When the temperature is increased, however, R_0A starts to increase over the fitted value, which is due to the reduced

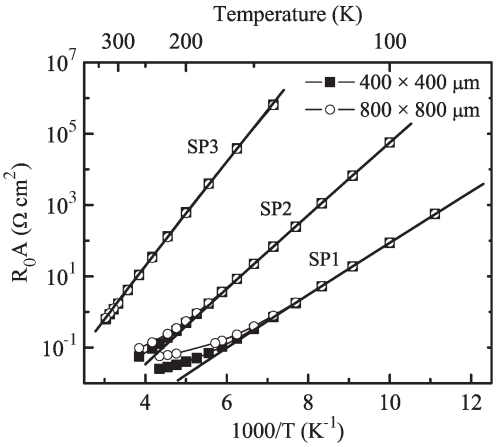

Fig. 2. Temperature-dependent R_0A for devices, as listed in Table I. The solid square and hollow circle data are for square-mesa devices with sizes of 400 and 800 μm, respectively. A fit to the low-temperature region (solid line) based on thermionic currents is extended to compare R_0A deviation at high temperatures.

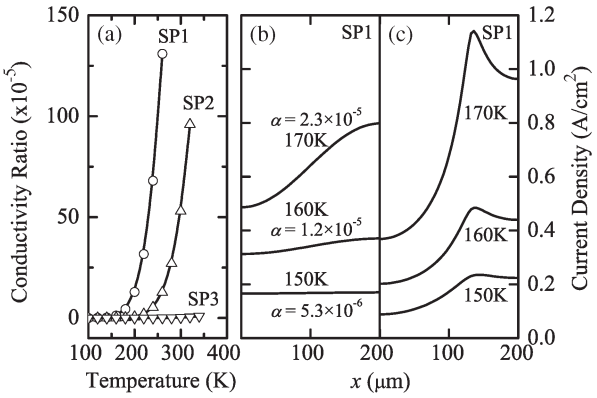

Fig. 3. (a) Relation of calculated conductivity ratio α with temperatures for all devices, where $\overline{\sigma}_z$ is obtained from fitting to low-temperature R_0A-T curves and $\overline{\sigma}_x$ calculated by using bulk parameters. (b) and (c) Calculated lateral current distributions for the device SP1 with the mesa 400 μm × 400 μm at the interface between the active region and bottom contact layer, and the interface between top contact layer and active region, respectively. $x = 0$ represents the device center. The nonuniformity becomes remarkable when the temperature is increased.

conduction area, i.e., currents become localized. This phenomenon is more prominent for devices with larger mesa sizes than that with smaller sizes.

The current nonuniformity originally results from the electric potential gradient in the lateral direction and depends on the conductivity ratio α as defined in (8). Fig. 3(a) shows the calculated $\alpha-T$ relationship for three samples, where $\overline{\sigma}_z$ is calculated by extrapolating the fitted line (Fig. 2) to the high-temperature region and $\overline{\sigma}_x$ is calculated using (9). Exponential increasing of α for SP1 takes place above 150 K, while SP3 has the same α with values close to zero over the entire temperature region up to 330 K. The only difference between samples is the Al fraction of barrier materials. This fact indicates critical effects of barrier height on the temperature behavior of α and R_0A deviation. It can be seen that the temperature for considerable change of α is consistent with that responsible for the beginning of R_0A deviation as shown in Fig. 2, which is defined as the threshold temperature T_t. A clear understanding of electrical characteristics regarding uniformity around T_t is to numerically calculate the 2-D current distribution. By using a finite-difference method and successive overrelaxation (SOR) iteration [14], the vertical current for the sample SP1 is calculated as a function of lateral position x and is shown in Fig. 3(b) and (c), which denotes the current at the interface between the active region and bottom contact layer, and at the interface between top contact layer and active region, respectively. The T_t of SP1 is 150 K. During calculation, three layers, i.e., active region, top bottom contact, and bottom contact, are separately evaluated with interface continuity of the electric potential and the vertical current flux between layers. The lateral component of conductivity for the active region are calculated using a formula similar to (9), but excluding the top and bottom layers, i.e., a weighted average of the bulk conductivities of emitters and barriers [11]. The boundary conditions are considered as $\partial\phi/\partial\vec{n} = 0$ on all surfaces without metal contacts, where $\vec{n}$ represents the normal direction of surfaces. Both current components in x and z directions can be obtained from solved electrical potential distribution. At 150 K, current is uniform over the entire lateral direction. However, nonuniformity with higher current at the device edge than that at the center appears when the temperature is increased to 160 and 170 K. Numerical calculations also verify not much difference of current profile below 150 K. Thus, a reduced conduction area is expected only when the temperature is increased above T_t. It can also be seen that the current uniformity at the interface between the top contact and the active region is worse than that at the interface between the bottom contact and the active region. This is a homogenizing effect of carrier transport after a long distance. Calculations illuminate the explanation for R_0A measurements based on the $\alpha-T$ relation in Fig. 3(a). Current localization results from the nonuniform electric potential being satisfied with the 2-D equation (7) and boundary conditions defined by the device geometry. The electric potential under the metal contact region, which lies at the device edge, becomes greater than that at the center. This nonuniformity induces reduced collection efficiency on carriers and, hence, the detector response since collection efficiency is related to the electrical potential difference. Fig. 4 shows that the relation between T_t and T_o (operating temperatures for optimum response) has been observed [7], as plotted in Fig. 4, where an additional sample with $\Delta = 74$ meV was used [6]. The agreement of T_t (defined from electrical performances) with T_O (defined from optical performances) indicates the importance of optimization of T_t for SO detectors. It can be seen that all samples approximately have the same value $\Delta/k_BT_t \approx 10$. This relation gives a simple selection rule of Δ for desired T_t or T_o. The increased phonon effect on the escape rate of excited carriers and SO absorption [15] could lead to a monotonic response increase with temperatures, as reported in the previous paper [6]. However, the nonuniformity appears in an exponential behavior of temperatures, which can be seen from calculated 2-D current distribution of the sample SP1 in Fig. 3(b) for 160 and 170 K (T_t is 150 K) operations. Therefore, a rapid degradation effect on response can be expected when the temperature is above T_t. These two

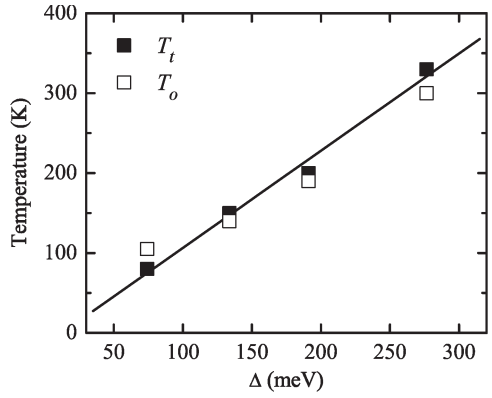

Fig. 4. Comparison of T_t and T_o versus thermal activation energy Δ. An additional sample with $\Delta = 74$ meV was used. T_t is the threshold temperature derived from Fig. 3(a), where a great change in α appears. T_o is the operating temperature for optimum response.

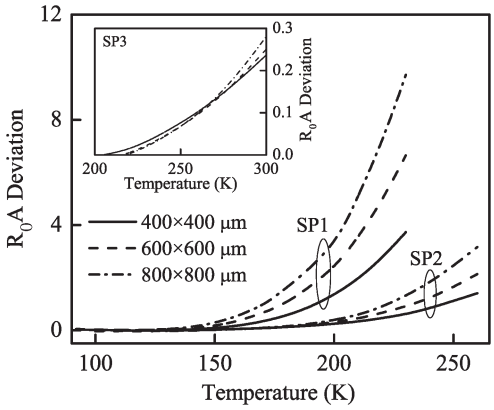

Fig. 5. Deviation of measured R_0A from that of the fitted value is defined as $(R_0A_{\text{measured}} - R_0A_{\text{fitted}})/R_0A_{\text{fitted}}$. The R_0A deviation becomes remarkable for samples with smaller Δ (SP1). The SP3 (inset) with the largest Δ exhibits little R_0A changes over the entire temperature region.

effects ultimately decide an operating temperature for optimum response.

The electrical nonuniformity is also related to device geometry. As the metal electrode lies at the edge of mesa, injected carriers must move forward the device center very quickly to realize uniform currents. At high temperatures, this process cannot be accomplished due to increased escape of carriers over the barrier. At this point, decreasing the mesa size will improve the uniformity. A clear view of device geometry effects on the R_0A product can be plotted by defining the deviation as $(R_0A_{\text{measured}} - R_0A_{\text{fitted}})/R_0A_{\text{fitted}}$, which is equivalent to the relative change from the uniform R_0A product value. Fig. 5 shows the temperature-dependent R_0A deviation. It can be seen that R_0A deviation is critical for devices with the larger mesa sizes.

Based on the theoretical model in Section III, two methods can be followed by either decreasing the vertical conductivity or increasing the lateral conductivity, both of which will reduce the conductivity ratio α. Increasing the barrier height can efficiently increase the uniformity as seen in Fig. 4. However, changing barrier height also shifts the threshold wavelength of detectors [7] and should be considered in the

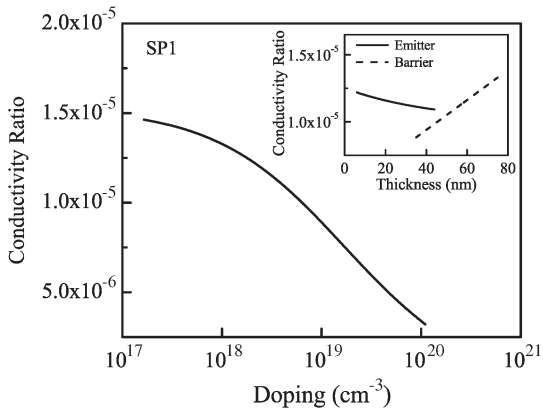

Fig. 6. Example of uniformity optimization for the device SP1 at 160 K by changing the emitter doping to decrease the conductivity ratio α. The inset is the dependence of α on the thickness of emitters and barriers.

overall optimization. The lateral conductivity [see (9)] can be increased by decreasing barrier thickness or increasing emitter thickness and doping, as shown in Fig. 6. Increasing emitter doping is beneficial since it increases optical absorption as well. However, the scattering effect [8] is another factor needed to be considered for a final optimized emitter. Detailed studies are in progress.

It should be noted that electrical nonuniformity of SO detectors was observed despite the fact that top and bottom layers are both highly p-doped $(1 \times 10^{19}\ \text{cm}^{-3})$. This is due to combined results of the conductivity anisotropy and the device geometry such as mesa sizes. As to devices in Fig. 1, the top contact layer (at the region of optical windows its thickness is 0.1 μm by partly etching) is not thick enough to uniformly spread carriers over long distance of devices (typical half-side length is 200 μm). Thus, the spreading of carrier is partly completed by involving the top layer of active region, which leads to nonuniformity. Theoretically, the nonuniformity can be decreased by reducing the mesa size. However, other factors could raise the issue of 2-D current transport as well. When devices operate at high electric field ($>$ 1 kV/cm), an exact form of drift velocity [see (3)], the image-force effect [10], and tunneling currents [1] should be considered. The vertical conductivity becomes bias dependent, i.e.,

$$\bar{\sigma}_z = \bar{\sigma}_z(V, T) \tag{11}$$

in which V denotes the bias applied on a single barrier. Under this situation, (7) should be numerically calculated in a self-consistent way, giving rise to strong narrowing of current profile [11], provided the vertical conductivity is increased with bias. As increased conductivity was measured in SO detectors (reasonably with the fact of thermal activation energy decreasing), remarkable nonuniformity will also be expected at high-bias operation. In addition, optical illumination is another factor that increases conductivity and changes the transport behavior of carriers. Therefore, 2-D analysis as stated above should be an important step for optimizing performances of high-operating-temperature infrared detectors.

V. Conclusion

A 2-D transport model has been investigated to explain experimental measurements on I–V–T characteristics of SO infrared detectors. The nonuniform behavior of the R_0A product was observed on devices with varied mesa sizes when the temperature is above a transition temperature T_t. The agreement of T_t with the operating temperature of detectors for optimum response is consistent with the result of the temperature-dependent transport mode of carriers in either 1- or 2-D characteristics. The increased vertical conductivity with temperatures is mainly responsible for the measured R_0A deviation. Better electrical uniformity for SO detectors working at high temperatures can be achieved by using smaller mesa sizes, higher doping in the p^+-GaAs region, and a higher potential barrier for SO detectors.

Acknowledgment

The authors would like to thank D. Kurkcuoglu for the initial experimental measurements.

References

[1] H. X. Yuan and A. G. U. Perera, "Dark current analysis of Si homojunction interfacial workfunction internal photoemission far-infrared detectors," *Appl. Phys. Lett.*, vol. 66, no. 17, pp. 2262–2264, Apr. 1995.

[2] H. C. Liu, A. G. Steele, M. Buchanan, and Z. R. Wasilewski, "Dark current in quantum well infrared photodetectors," *J. Appl. Phys.*, vol. 73, no. 4, pp. 2029–2031, Feb. 1993.

[3] J. Y. Andersson, "Dark current mechanisms and conditions of background radiation limitation of n-doped AlGaAs/GaAs quantum-well infrared detectors," *J. Appl. Phys.*, vol. 78, no. 10, pp. 6298–6304, Nov. 1995.

[4] D. G. Esaev, M. B. M. Rinzan, S. G. Matsik, and A. G. U. Perera, "Design and optimization of GaAs/AlGaAs heterojunction infrared detectors," *J. Appl. Phys.*, vol. 96, no. 8, pp. 4588–4597, Oct. 2004.

[5] B. F. Levine, C. G. Bethea, G. Hasnain, V. O. Shen, E. Pelve, R. R. Abbott, and S. J. Hsieh, "High sensitivity low dark current 10 μm GaAs quantum well infrared detector," *Appl. Phys. Lett.*, vol. 56, no. 9, pp. 851–853, Feb. 1990.

[6] A. G. U. Perera, S. G. Matsik, P. V. V. Jayaweera, K. Tennakone, H. C. Liu, M. Buchanan, G. Von Winckel, A. Stintz, and S. Krishna, "High operating temperature split-off band infrared detectors," *Appl. Phys. Lett.*, vol. 89, no. 13, pp. 131 118-1–131 118-3, Sep. 2006.

[7] P. V. V. Jayaweera, S. G. Matsik, A. G. U. Perera, H. C. Liu, M. Buchanan, and Z. R. Wasilewski, "Uncooled infrared detectors for 3–5 μm and beyond," *Appl. Phys. Lett.*, vol. 93, no. 2, pp. 021 105-1–021 105-3, Jul. 2008.

[8] S. G. Matsik, P. V. V. Jayaweera, A. G. U. Perera, K. K. Choi, and P. Wijewarnasuriya, "Device modeling for split-off band detectors," *J. Appl. Phys.*, vol. 106, no. 6, pp. 064 503-1–064 503-6, Sep. 2009.

[9] H. Schneider and H. C. Liu, *Quantum Well Infrared Photodetectors: Physics and Applications*. New York: Springer-Verlag, 2007.

[10] A. G. U. Perera, H. X. Yuan, and M. H. Francombe, "Homojunction internal photoemission far-infrared detectors: Photoresponse performance analysis," *J. Appl. Phys.*, vol. 77, no. 2, pp. 915–924, Jan. 1995.

[11] A. Lyakh, P. Zory, D. Wasserman, G. Shu, C. Gmachl, M. D'Souza, and D. Botez, "Narrow stripe-width, low-ridge high power quantum cascade lasers," *Appl. Phys. Lett.*, vol. 90, no. 14, pp. 141 107-1–141 107-3, Apr. 2007.

[12] S. G. Matsik and A. G. U. Perera, "Self-consistent performance modeling for dualband detectors," *J. Appl. Phys.*, vol. 104, no. 4, pp. 044 502-1–044 502-10, Aug. 2008.

[13] H. X. Yuan and A. G. U. Perera, "Space-charge-limited conduction in Si n^+-i-n^+ homojunction far-infrared detectors," *J. Appl. Phys.*, vol. 79, no. 8, pp. 4418–4425, Apr. 1996.

[14] R. L. Burden, J. D. Faires, and A. C. Reynolds, *Numerical Analysis*. Boston, MA: Prindle Weber & Schmidt, 1981.

[15] G. N. Childs, S. Brand, and R. A. Abram, "Intervalence band absorption in semiconductor laser materials," *Semicond. Sci. Technol.*, vol. 1, no. 2, pp. 116–120, Aug. 1986.

Y. F. Lao received the B.S. and M.S. degrees in physics from Zhejiang University, Hangzhou, China, in 1999 and 2002, respectively, and the Ph.D. degree in microelectronics and solid-state electronics from the Shanghai Institute of Microsystem and Information Technology, Shanghai, China, in 2007.

He is currently a Postdoctoral Researcher with the Department of Physics and Astronomy, Georgia State University (GSU), Atlanta, working on infrared detectors based on the split-off band transition and theoretical modeling. His current research interest includes semiconductor optoelectronics. His work has been focused on the molecular beam epitaxial growth of III–V semiconductor compounds and the vertical-cavity surface-emitting lasers.

P. V. V. Jayaweera received the B.S. degree in physics special from the University of Sri Jayewardenepura, Nugegoda, Sri Lanka, in 1999 and the M.S. and Ph.D. degrees from Georgia State University (GSU), Atlanta, in 2007 and 2009, respectively.

He is currently a Senior Scientist with the SPD Laboratory Inc., Hamamatsu, Japan. He is the author or a coauthor of over 26 technical papers in archival journals. He is the holder of a patent. His research interests include photon detection techniques and development of low-cost photovoltaic cells as a renewable energy source.

Dr. Jayaweera was the Recipient of the Outstanding Advanced Graduate Student (Physics) Award in 2007 presented by the Department of Physics, GSU.

Steven G. Matsik received the B.S. degree from Wake Forest University, Winston-Salem, NC, in 1979 and the M.S. and Ph.D. degrees from Georgia State University (GSU), Atlanta, in 1996 and 1998, respectively.

He is currently with the Department of Physics and Astronomy, GSU. He is the author of more than 20 published articles. His research interests includes the development of semiconductor optoelectronic devices.

Dr. Matsik received the Outstanding Senior Graduate Student Award at GSU.

A. G. Unil Perera (SM'03) obtained the B.S. degree (Physics Special, First-Class Honors) from the University of Colombo, Colombo, Sri Lanka and the M.S. and Ph.D. degrees from the University of Pittsburgh, Pittsburgh. PA.

He is currently an Associate Chair with the Department of Physics and Astronomy and is also the Graduate Director of the Physics program at Georgia State University (GSU), Atlanta. As a Professor of physics at GSU, his focus is on developing multiband and terahertz photon detectors. He has participated in several "advanced research workshops and has presented invited talks at many conferences. He is the author of written six book chapters and has contributed to the CRC dictionary of electronics, is a coeditor of a volume on thin-film optical devices for a five-volume handbook, has served on National Science Foundation, Department of Energy, and National Aeronautic and Space Administration review panels and as a reviewer for numerous research proposals and papers. He is the author of over 125 published technical articles. He is the holder of five patents (or applications). His work was featured in various professional journals such as *Laser Focus World, Photonics Spectra* and *Reviews of Modern Physics*.

Dr. Perera is a Fellow of the American Physical Society and a Fellow of the Society of Photo-Instrumentation Engineers.

H. C. Liu (M'99–SM'05–F'07) was born in Taiyuan China. He received the B.Sc. degree in physics from Lanzhou University, Lanzhou, China, in 1982 and the Ph.D. degree in applied physics from University of Pittsburgh, Pittsburgh, PA, in 1987, as an Andrew Mellon Predoctoral Fellow.

He was the overseas Changjiang Chair Professor at the Shanghai Jiaotong University, Shanghai, China, in 2008. He is currently the Imaging Devices Group Leader with the Institute for Microstructural Sciences, National Research Council of Canada, Ottawa, ON, Canada. He is the author and a coauthor of about 350 refereed journal articles (with about 90 first or sole authored) and has given 120 talks (80 invited) at international conferences. He is the holder of over a dozen patents. His major research interest is semiconductor quantum devices.

Dr. Liu has been elected as a Fellow of the Academy of Sciences—Royal Society of Canada and a Fellow of the American Physical Society. He received the Herzberg Medal from the Canadian Association of Physicists in 2000, the Bessel Prize from the Alexander von Humboldt Foundation in 2001, and the Chinese Oversea Distinguished Young Scientist Award (NSFC-B) in 2005.

M. Buchanan received the B.Sc. degree in physics from the University of Manitoba, Winnipeg, MB, Canada, in 1965 and the Ph.D. degree in solid-state physics from McMaster University, Hamilton, ON, Canada, in 1969.

She joined the National Research Council of Canada, Ottawa, ON, Canada, in 1975 and, after working in the Division of Physics and the Division of Energy, joined the Institute for Microstructural Sciences in 1985 as one of a group of three developing the semiconductor device fabrication facilities. She served as Group Leader for the Nanofabrication Group for eight years. She is the author or coauthor of more than 290 papers and conference proceedings.

Z. R. Wasilewski received the Ph.D. degree from the Institute of Physics, Polish Academy of Sciences, Warsaw, Poland, in 1986. His doctoral work focused on the influence of high hydrostatic pressure on the magnetooptical properties of shallow and deep donors in InSb.

He joined the National Research Council of Canada, Ottawa, ON, Canada, in 1988 after one year of Postdoctoral Fellowship with the Imperial College of Science and Technology, London, U.K. Since 1989, his work has been focused primarily on the molecular beam epitaxial growth and characterization of III–V semiconductor compounds. He is currently the Principal Research Officer in the Epitaxial and Multilayer Materials of the Institute for Microstructural Sciences, National Research Council of Canada. He is a coauthor of over 350 refereed journal articles and conference proceedings.